Theor Chem Acc (1998) 100:65–77
DOI 10.1007/s002149800m71

Theoretical
Chemistry Accounts

Regular article

Dissociative recombination of HeH^+. I. Rovibrational spectrum of HeH Rydberg states*

Wolfgang P. Kraemer[1], **Per-Åke Malmqvist**[2]

[1]Max Planck Institute for Astrophysics, P. O. Box 1523, D- 85740 Garching, Germany
[2]Department of Theoretical Chemistry, Chemical Center, P. O. Box 124, University of Lund, S-221 00 Lund, Sweden

Received: 22 June 1998 / Accepted: 21 August 1998 / Published online: 12 October 1998

Abstract. The repulsive ground electronic state $X^2\Sigma^+$ of HeH is strongly coupled to the Rydberg states at small interatomic distances. Such large couplings also occur between some of the Rydberg states. HeH^+ ions that capture an electron in a Rydberg state end up in separated He and H atoms by indirect predissociation. This paper presents a study of potential functions and pertinent matrix elements involving the lowest electronic states: the $^2\Sigma^+$ states, X, A, C, and D, and the $^2\Pi$ states B and E. Individual transition rates as well as total radiative and non-radiative lifetimes have been computed for the lowest vibrational and rotational levels.

Key words: Dissociative recombination – HeH Rydberg states – Adiabatic corrections – Diabatic coupling – Radiative and non-radiative reaction rates

1 Introduction

The small two-electron ion HeH^+ is of considerable astrophysical interest due to its predicted presence in many interstellar environments. In the primordial gas, for instance, the initial formation of the ion is assumed to have occurred in a radiative association process either in the direct single-state reaction

$$He + H^+ \rightarrow HeH^+(X^1\Sigma^+) + h\nu \qquad (1)$$

or in the two-state reaction

$$He^+ + H \rightarrow HeH^+(A^1\Sigma^+) \rightarrow HeH^+(X^1\Sigma^+) + h\nu \ , \qquad (2)$$

whereas the most efficient depletion of the ion in this environment is most likely via dissociative recombination (DR) with electrons according to

$$HeH^+(X^1\Sigma^+) + e \rightarrow He + H \ . \qquad (3)$$

DR has been known for many years [1] to be a fast process if the ground electronic state potential of the molecular ion is crossed close to its minimum by the repulsive potential of an appropriate neutral unstable state which is assumed to have a doubly excited electronic configuration relative to the initial (ion + continuum electron) state in order to explain the removal of the kinetic energy of the captured electron [2]. This mechanism is usually called the direct process and many of the DR reactions for which large reaction rate constants have been measured were therefore assumed to proceed according to this mechanism [3]. Recently it was recognized [4], however, that the occurrence of a suitable potential curve crossing close to the minimum of the potential is not a necessary condition for the efficiency of the process. Considering, for example, a number of small molecular ions such as HeH^+, H_3^+, and HCO^+, which are all of prime astrophysical interest and for which fairly large DR reaction rate constants were measured using different experimental setups, it is possible to demonstrate on the basis of extensive ab initio calculations that for all these ions suitable curve crossings do not exist [5–7]. It has been shown instead that single-electron radiationless transitions within the sequence of associated Rydberg states can efficiently replace the corresponding two-electron transitions which control the direct crossing mode mechanism [8]. In this so-called indirect or tunneling mode mechanism the DR reaction is driven by the kinetic energy operator, i.e., through the coupling of the nuclear motion with the electronic continuum, which indicates the breakdown of the Born-Oppenheimer approximation for this reaction mechanism [9–11]. In the direct process the incoming colliding electron is captured into a dissociating valence state which has practically very little coupling to the electronic continuum and the Rydberg states of the same symmetry. The potential of this state and its properties can therefore be reasonably well described within the Born-Oppenheimer approximation scheme. In the indirect process, however, electron capture takes place into the Rydberg states converging to the ion limit and the efficiency of the dissociative stabilization of the capture step depends on the strength of the couplings between the Rydberg states and the coupling to a possibly available dissociative state.

* Dedicated to Prof. Dr. Wilfried Meyer on the occasion of his 60th birthday

Correspondence to: W. P. Kraemer

The essential features of these interactions are of "non-Born-Oppenheimer" type and apart from detailed knowledge of the character of the relevant Rydberg states and their adiabatic corrected potentials, a quantitative description of the indirect process therefore also requires evaluation of the non-adiabatic coupling terms.

In the HeH^+/HeH system the ion in its ground electronic state dissociates to $He + H^+$ with a dissociation energy, D_e of only 16448.4 cm^{-1}. The neutral species has a repulsive ground electronic state $X^2\Sigma^+$ with a shallow van der Waals minimum [12] and above this state a series of bound excited Rydberg states exists, converging toward the lowest ionization limit. These states correlate on dissociation with the $H(ns)$ asymptote with $n = 1, 2, 3$. In the commonly accepted nomenclature these states are in Σ^+ symmetry the X, A, C, D, F, and I states, in Π symmetry the B, E, and H states, and finally the $1^2\Delta$ or G state. In previous ab initio calculations it was stated [13] that there are no avoided curve crossings among these states, but that rather strong radial couplings via the nuclear kinetic energy operator exist and that due to these couplings the excited Rydberg states are easily depopulated by either radiative emission or predissociation processes. The present calculations, however, show very clearly that there is actually an avoided curve crossing between the D and F states at the internuclear distance $R = 2.2a_0$ which is manifested by the strongly peaked adiabatic correction of the Born-Oppenheimer potential in this region.

After the first theoretical prediction of the existence of stable excited Rydberg states of HeH in 1963 by Michels and Harris [5], which was confirmed later by several other ab initio calculations, the HeH molecule gained considerable attention among experimentalists and theoreticians because of fundamental interest in this most simple excimer system and also because it is regarded as an ideally suited model system for making direct comparisons between experiment and theory. Rather complete coverage of previous experimental and theoretical work on the spectroscopy of the HeH Rydberg states and their depopulation processes is provided in Refs. [14, 15].

The present study is the first in a forthcoming series of studies of DR processes of small molecular ions of astrophysical interest employing ab initio quantum chemical methods for studying the reaction energetics, and especially making use of the restricted active space state interaction (RASSI) method for evaluating the couplings between the (ion + continuum electron) and the electron capture states. Since the HeH^+ + electron DR process proceeds according to the indirect reaction mechanism, the present study is concerned with the spectroscopy of the HeH Rydberg states and their radiative emission and predissociation properties. The potential energies of the HeH states were calculated within the Born-Oppenheimer approximation at the multi-reference configuration interaction (MRCI) level of theory, whereas adiabatic corrections to the potentials and non-adiabatic couplings between the states were determined from *restricted active space* self-consistent field (RASSCF) wave functions. For this system, the RASSCF calculations are quite accurate. For the present three-electron system a full configuration interaction (FCI) treatment could have been applied throughout. However, since the same kind of calculations will also be done for larger systems, it was decided to do the calculations on the present approximation level.

The present study describes calculations of the spectroscopic constants for the six lowest bound excited Rydberg states of HeH and the radiative lifetimes of the lower vibrational levels using presently calculated adiabatic potentials including adiabatic corrections and it also presents calculations of the total radiative transition rates obtained directly by contour integration as well as non-radiative transition rates computed from Golden Rule matrix elements over adiabatic wave functions. In contrast to the previous study by van Hemert and Peyerimhoff [14] which includes only the D/C radiative transition and the A/X predissociation, the present study offers a complete set of data for all possible transitions within the lowest six states of HeH. In a very recent study by Vegiri [16], on the other hand, who performed a similar complete investigation of all possible transitions it appears that usage was made of some coupling data computed earlier by Petsalakis et al. [17, 18] which were found here to be not very reliable. In this situation it seems to be well-justified that in the present study another attempt is made to provide a complete and consistent analysis of the lower HeH Rydberg states.

2 Methods

2.1 Basis sets

It is often fairly easy to get relative energies correct for the lowest Rydberg states, since they have a positive ion core in common and the Rydberg electron introduces only minor correlation effects. The necessary extra diffuse basis functions can usually be designed by a rule of thumb: a small set of extra primitive Gaussians are chosen with maxima at the same radial distance as the hydrogenic wave functions, and an additional set is chosen with maxima somewhere between these values. (The second set is necessary in order to achieve the flexibility that allows optimized quantum defects.) In the present case, we want to determine accurate coupling matrix elements as well as energies. Therefore, a more elaborate optimization procedure was used.

Furthermore, all the excited electronic states considered in this study dissociate into ground state He and an excited H atom (see Fig. 1). This causes a qualitative difference between the exact adiabatic wave functions and those computed by a standard LCAO aproach with any Gaussian basis. At some finite distance, the computed wave functions change character fairly abruptly. Asymptotically, they describe the excited H atom as having fairly pure s, p, or d character. At shorter distances, they change over to represent the static dipolar hydrogenic states (the "parabolic states" unique to a hydrogenic atom), with the large static dipole moment coupled to a polarized He atom. Since the components of the hydrogenic main shells are exactly degenerate, the exact adiabatic wave functions do not show such a switch in character at any finite distance. We do not

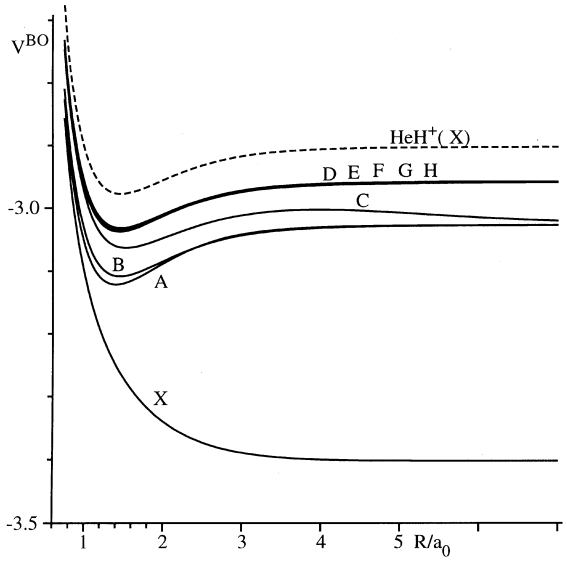

Fig. 1. Potential curves of the HeH^+ ground state and the lowest states of HeH

want to have to worry about the effects of the non-physical switching from dipolar to unpolarized character, and we thus want to allow the basis set to describe hydrogenic main shells which are accurately degenerate.

We started with a conventional atomic natural orbital (ANO) basis set, which is able to give reasonably good results, including correlation, for valence states of neutral HeH and for the HeH^+ ion core. An additional basis set was designed by calculations on hydrogenic one-electron problems as follows. For any given set of primitive Gaussians, the exact 1*s* function was projected away, and a calculation was made for the lowest states. The basis set parameters were optimized for the lowest possible sum of energies. By projecting away the 1*s* orbital, we express our assumption that the basis functions are to be used in addition to a conventional valence basis set. (If this is not done, optimization of the 1*s* functions may well dominate the procedure and give too contracted basis functions. After optimization it will also be difficult to separate the innermost basis functions and replace them with the conventional basis.) In order to achieve the flexibility for quantum defects, the calculation also included a non-physical poblem, with 1/2 added to the angular quantum number, representing roughly half-integer values of the effective main quantum number. A Rydberg basis of ANO type, with a 5*s*, 5*p*, 3*d*, and 2*f* function was finally chosen. With this basis set, the largest energy error for hydrogenic Rydberg states, with $n = 1-4$, was 0.0004 a.u. and occurred for the 4*d* state. The basis set and the optimizer can be obtained from the authors.

2.2 Calculation of electronic states

For the electronic structure calculations, we used the MOLCAS [19] suite of programs with some modifications.

Adiabatic electronic states were computed by two different programs: for the potential functions, we used the MRCI program of Siegbahn and Blomberg [20], while adiabatic corrections to the potential and non-adiabatic coupling matrix elements were computed from RASSCF wave functions [21, 22].

Obviously, for a three-electron problem, it would make sense to use the FCI method instead for all quantities. For larger systems, however, it is preferable to use the RASSCF method, since then we can easily compute any matrix elements even with separately optimized wave functions. On the other hand, the RASSCF method cannot give as high accuracy for the potentials as an MRCI calculation.

For wave functions of the RASSCF type, matrix elements of one-electron and two-electron operators can be very rapidly computed, given the one-electron or two-electron integrals of the operators over the AO basis set. This is also just as easy if the bra and the ket side use different orbitals, and if the orbitals (and thus the basis functions for the CI wave function, i.e., the configuration functions) are non-orthogonal [23, 24]. A program called RASSI [25] in the MOLCAS package was modified for our purposes, so that it could compute arbitrary matrix elements of the following types:

$$\langle\psi_1|\hat{A}|\psi_2\rangle$$
$$\langle\psi_1|\hat{A}|\partial/\partial Q_p\psi_2\rangle$$
$$\langle\psi_1|\hat{A}|\partial^2/\partial Q_p\partial Q_q\psi_2\rangle \ ,$$

where $\hat{A}$ is any one-electron operator for which integrals can be provided. The independent variables Q_p, Q_q are arbitrary linear combinations of cartesian coordinates in the coordinate frame used for the electronic calculations. Derivatives of AO integrals were computed by numerical differentiation. These matrix elements can also be computed if $\hat{A}$ is the two-electron part of a product of two such one-electron operators.

In the present investigation, we needed only two matrix elements involving differentiation, namely $\langle\psi_1|\partial/\partial R\psi_2\rangle$ and $\langle\psi_1|\partial^2/\partial R^2\psi_2\rangle$. We also computed matrix elements of the one-electron operators $\hat{\mu}_x$, $\hat{\mu}_z$, $\hat{L}_y$, $\hat{L}_z$, $\hat{P}_x$, and $\hat{P}_z$, and of the two-electron operators $\hat{\mathbf{L}}^2$ and $\hat{\mathbf{P}}^2$ in the conventional way. Here, μ is the electronic dipole moment operator, $\hat{\mathbf{L}}$ is the electronic angular momentum, $\hat{\mathbf{P}}$ is the electronic linear momentum, and the molecule is oriented along the *z*-axis. The use of these quantities will be described later.

For the calculation of the matrix elements, our present implementation assumes that the qualitative structure of the bra and ket wave functions are the same: they have the same number of inactive, RAS-1, RAS-2, RAS- 3, and virtual orbitals. The RASSCF calculations have therefore been subdivided into two steps each: a preliminary calculation, which serves only as an orbital generator, and a second step, which only performs the CI without orbital reoptimization, which we will call a RASCI calculation.

In the RASCI step, there are no inactive orbitals, and the active orbital space comprises 19 orbitals. These are subdivided into 5 RAS-2 and 14 RAS-3 orbitals (there is no RAS-1 in this case), and at most two electrons are allowed in the RAS-3 space. Thus, the RAS-2 space is always occupied by at least one electron. Schematically, it contains the He 1s, 2s, 2p_z orbitals of σ symmetry, and the He 2$p_{x,y}$ orbitals of symmetry π_x and π_y. The RAS-3 orbital space is occupied by at most two electrons and contains the hydrogenic Rydberg orbitals with $n = 1$–3. There are 5σ, 3π and 1δ functions, the latter two having two components each. The calculation was actually done using real orbitals in C_{2v} rather than $C_{\infty v}$ symmetry, with equivalence of π components enforced.

The above description of the orbital character is oversimplified in several respects: it is valid only for long distances, so the characterization should be taken in the sense of a correlation to the dissociation limit. Also, within each main shell the indicated AO's actually mix, as already mentioned, to form "parabolic" states with a static dipole moment along the z-axis. Finally, they are obviously not unperturbed atomic functions, nor selected for their approximate atomic character, but have been obtained from the orbital optimization RASSCF step.

This preliminary RASSCF calculation differed for four different cases. These were: the ground state; the average of the first seven states in A_1 (which comprised the ground state, five Rydberg sigma states, and one delta state); the average of the three lowest states of symmetry B_2 (three Rydberg $^2\Pi$ states); and the lowest state of symmetry A_2 (a delta state, symmetricly equivalent to the one in symmetry A_1).

For the ground state, we used a CASSCF calculation with six active orbitals: four a_1, one b_2, and one b_1 (the latter are actually equivalent). Quasicanonical orbitals are formed: those that diagonalize a Fock matrix, but allowing only actives to mix with actives, and virtuals with virtuals. In symmetry a_1, these orbitals form the sequence He 1s, H1s, He2s, He2p_z, H2s..., which is then reordered in the proper sequence for the RASCI step.

Similarly, to produce any other state with optimized orbitals, and then rearrange to fit the RASCI scheme, takes some forethought and is tedious to describe in full detail. Of course, once the whole procedure was set up, it ran automatically through all calculations. A more detailed description may be obtained from the authors.

Since matrix elements involving the derivative of wave functions were calculated by numeric differentiation, the phase of orbitals and CI coefficients must be controlled. The necessary continuity was in almost all cases guaranteed by the use of neighboring results for restarting the RASSCF calculation at the next point. However, it also became necessary to monitor the results from several calculations to make sure that relative phases were correct: for instance, $\langle i|\partial/\partial R|j\rangle$ should be close to $-\langle j|\partial/\partial R|i\rangle$. The first matrix element was computed, for all states $|i\rangle$, with a differentiated wave function $\partial/\partial R|j\rangle$, and the second element was produced in another sequence of calculations, where $|i\rangle$ was differentiated. Unless the relative phase of all states in each calculation is monitored, there is a risk that non-diagonal matrix elements will have spurious sign changes. In fact, it seems that the matrix elements of Refs. [17, 18], which have been used in several studies, contain this type of error.

All matrix elements were computed for bra states dissociating to the $n = 1, 2, 3$ manifold, conventionally named X, A, B, C, D, E, F, G, H, and I. The ket side, which was the differentiated state, has so far been evaluated only for the states X up to E. Thus, adiabatic corrections can only be evaluated for this subset of states.

2.3 Calculation of rotational and vibrational states

The wave function is assumed to have the form

$$|N\Lambda vn\rangle = \sqrt{\frac{2N+1}{4\pi}}\, d^{(N)}_{N_z\Lambda}(\theta)\exp(iN_z\phi)\chi_{v\Lambda}(R) \times \Phi^{\mathrm{el}}_{\Lambda n}(R;\ldots,\mathbf{r}'_k,\ldots)\ . \tag{4}$$

The total angular momentum, excluding spin, is $\hat{\mathbf{N}}$. It is an eigenfunction of $\hat{\mathbf{N}}^2$, its projection on the laboratory z-axis $\hat{N}_z$, and its projection on the molecular axis $\hat{N}_e$. The eigenvalues are $N(N+1)$, N_z, and Λ, where Λ is identical to the electronic angular moment component along the axis. The electronic coordinates, $\ldots,\mathbf{r}'_k,\ldots$ are defined using the molecule-fixed coordinate frame.

With this wave function, the Hamiltonian is

$$\hat{H} = -\frac{1}{2m_{12}}\left(\frac{\partial^2}{\partial R^2} - \frac{1}{R^2}\left(\hat{\mathbf{N}}-\hat{\mathbf{L}}\right)^2\right) - \frac{1}{2(m_1+m_2)}\sum_{ij}\nabla_{\mathbf{r}'_i}\cdot\nabla_{\mathbf{r}'_j} + \hat{H}^{\mathrm{el}}\ , \tag{5}$$

where the electronic Hamiltonian $\hat{H}^{\mathrm{el}}$ includes the internuclear repulsion energy, and the integration element is

$$\sin\theta\, dR\, d\theta\, d\phi \prod_k d\mathbf{r}^3_k\ . \tag{6}$$

The electronic wave function depends on the orientation and magnitude of $\mathbf{R}$, so this simple Hamiltonian has somewhat complicated matrix elements, with, for example, terms produced by $|\partial/\partial R$ acting on the electronic wave function. If such terms are ignored, the usual Born-Oppenheimer approximation is obtained, with a potential function for nuclear motion, $V^{\mathrm{BO}}_{\Lambda n}(R)$, given by the expectation value of the electronic Hamiltonian integrated only over electron coordinates, for any given nuclear coordinates. Corrections are defined in terms of the following matrices:

$$A^{\Lambda}_{n'n}(R) = \left\langle \Lambda n'\left|\frac{\partial}{\partial R}\right|\Lambda n\right\rangle_{\mathrm{el}} \tag{7}$$

$$B^{\Lambda}_{n'n}(R) = \left\langle \Lambda n'\left|\frac{\partial^2}{\partial R^2}\right|\Lambda n\right\rangle_{\mathrm{el}} \tag{8}$$

$$C^{\Lambda}_{n'n}(R) = \left\langle \Lambda n' \left| \frac{\hat{\mathbf{L}}^2}{R^2} \right| \Lambda n \right\rangle_{\mathrm{el}} \tag{9}$$

$$Q^{\Lambda}_{n'n}(R) = \left\langle \Lambda + 1 n' \left| \frac{\hat{L}^+}{R} \right| \Lambda n \right\rangle_{\mathrm{el}} \tag{10}$$

$$D^{\Lambda}_{n'n}(R) = \left\langle \Lambda n' \left| \frac{\hbar^2}{2} \sum_{ij} \nabla_i \cdot \nabla_j \right| \Lambda n \right\rangle_{\mathrm{el}} \quad . \tag{11}$$

These matrices may be called the radial first derivative matrix, the radial second derivative matrix, the angular second derivative matrix, the rotational coupling matrix, and finally the mass polarization matrix.

With a basis of state functions defined as in Eq. (4), the non-zero Hamiltonian matrix elements are

$$\begin{aligned}\left\langle N\Lambda v' n' | \hat{H} | N\Lambda v n \right\rangle &= \delta_{n'n} \int \chi^*_{v'\Lambda}(R) V^{\mathrm{BO}}_{\Lambda n} \chi_{v\Lambda}(R) dR \\ &- \frac{\hbar}{2m_{12}} \int \chi^*_{v'\Lambda}(R) \left(\frac{\partial^2}{\partial R^2} + 2A^{\Lambda}_{n'n}(R) \frac{\partial}{\partial R} + B^{\Lambda}_{n'n}(R) \right) \\ &\qquad \times \chi_{v\Lambda}(R) dR \\ &+ \frac{\hbar}{2m_{12}} \int \chi^*_{v'\Lambda}(R) \left(C^{\Lambda}_{n'n}(R) \right) \chi_{v\Lambda}(R) dR \\ &- \frac{\hbar^2}{2(m_1 + m_2)} \int \chi^*_{v'\Lambda}(R) (D^{\Lambda}_{n'n}(R)) \chi_{v\Lambda}(R) dR \end{aligned} \tag{12}$$

and

$$\begin{aligned}&\left\langle N\Lambda + 1 v' n' | \hat{H} | N\Lambda v n \right\rangle = \\ &\frac{h^2}{2m_{12}} \sqrt{\frac{(N-\Lambda)(N+\Lambda+1)}{R}} \\ &\int \chi^*_{v'\Lambda+1}(R) (Q^{\Lambda}_{n'n}(R)) \chi_{v\Lambda}(R) dR \quad . \end{aligned} \tag{13}$$

We do not consider spin, so N and N_z are good quantum numbers. For any given electronic state Λn, the diagonal elements of the matrices **B**, **C**, and **D** define the adiabatic correction to the Born-Oppenheimer potential function:

$$V^{\mathrm{BODC}}_{\Lambda n} = V^{\mathrm{Rad}}_{\Lambda n} + V^{\mathrm{Ang}}_{\Lambda n} + V^{\mathrm{MP}}_{\Lambda n} \tag{14}$$

$$V^{\mathrm{Rad}}_{\Lambda n} = -\frac{\hbar^2}{2m_{12}} B^{\Lambda}_{nn}(R) \tag{15}$$

$$V^{\mathrm{Ang}}_{\Lambda n} = \frac{\hbar^2}{2m_{12}} C^{\Lambda}_{nn}(R) \tag{16}$$

$$V^{\mathrm{MP}}_{\Lambda n} = -\frac{\hbar^2}{2(m_1 + m_2)} D^{\Lambda}_{nn}(R) \quad . \tag{17}$$

Wave functions for the nuclear motion were obtained by solving the radial Schrödinger equation in a finite element approximation. This implies using a variational method, with basis functions (the "elements") consisting of piecewise polynomials, each represented simply by their value at particular points on each grid interval. As has been shown by Light *et al.* [26, 27], by using the proper evaluation points for a Gauss integration scheme, the resulting equation solver is as simple as the usual difference approximation schemes. If the potentials were piecewise polynomials, the integrals would be exact. The only approximations are thus the incompleteness of the basis and the resulting inaccurate representation of the potential as a piecewise polynomial. In our implementation, the joints between the finite elements – the knots – are included in the evaluation points. The remaining points and the integration weights are designed to give exact integrals for piecewise polynomials with values continuous across knots. This is equivalent to using Lobatto's integration formula rather than the Gauus one.

The potential and other functions of the interatomic distance were interpolated as spline functions in an auxiliary variable r^{-k}, where the exponent $-k$ depended on the physical quantity being represented. These spline functions were first fitted to the few (typically 37) points evaluated by the quantum chemical calculations. They were later evaluated at the proper grid points for the Gauss-Lobatto quadrature for the nuclear Schrödinger equation. Calculations were done with the Born-Oppenheimer potential V^{BO} or with the adiabatic potential $V^{\mathrm{BO}} + V^{\mathrm{BODC}}$.

2.4 Calculation of radiative and non-radiative rates

Radiative rates in the dipole approximations are commonly obtained using either the dipole length or the dipole velocity forms. Dipole and velocity matix elements over the electronic state functions were computed by the RASSI program, which allows the states to be expressed in separately optimized molecular orbitals. Only the dipole matrix elements were finally used to compute radiative rates, but early calculations showed that the two forms gave excellent agreement, within a few percent, except when two levels were very close. For individual transitions, the radiation emission rate is expressed by Einstein's coefficient A_{fi}:

$$A_{fi} = \tau_0^{-1} 2\alpha^3 (\Delta E_{fi}/E_h)^2 f_{fi} \quad , \tag{18}$$

where τ_0 is the atomic time unit, E_h is the atomic energy unit (1 Hartree), and α is the fine structure constant. $\tau_0 = \hbar/E_h$ is $24.188\,843 \times 10^{-18}$ s, E_h is 219474.64 cm^{-1}, and α is 1/137.035 989. f_{fi} is the dimensionless oscillator strength,

$$\begin{aligned} f_{fi} &= S(\Delta N N' \Delta\Lambda') \left(\frac{2}{3} \frac{m_e}{\hbar^2 e^2} \right) \Delta E_{fi} \\ &\qquad \times \left| \int \chi_f(R)^* \mu(R) \chi_i(R) dR \right|^2 \quad , \end{aligned} \tag{19}$$

where $S(\Delta N N' \Delta\Lambda')$ is the Hönl-London factor, and $\mu(R)$ is a component of the electronic dipole matrix element over the electronic state functions. The change in N quantum number can only be $\Delta N = -1, 0$, or 1, conventionally indicated by letters P, Q, and R. The change in Λ can also only be $-1, 0$, or 1, and determines which component of the electronic dipole moment is used.

The total radiative rate for a given level can be written as

$$k_i = \int\limits_{E_f<E_i} A_{fi} D(E_f) dE_f \ , \tag{20}$$

where $D(E)$ is the density of states. It is convenient to partition this into a sum of partial rates, one for each final electronic state. Using atomic units for simplicity, this becomes an integral

$$k_i = \frac{4\alpha^3}{3\tau_0} \int\limits_{\epsilon=0}^{\infty} \epsilon^3 \langle \psi_i | \hat{\boldsymbol{\mu}} \hat{P}(E_i - \epsilon) \hat{\boldsymbol{\mu}} | \psi_i \rangle d\epsilon \ , \tag{21}$$

where $\hat{P}(E)dE$ is a projector onto states with energy in the interval $[E, E + dE]$.

Using Gauss' integration formula, we may reexpress this as a contour integral.

$$k_i = \frac{4\alpha^3}{3\tau_0} \left(\frac{i}{2\pi}\right) \oint (E_i - z)^3 \langle \psi_i | \hat{\boldsymbol{\mu}} (\hat{H} - z)^{-1} \hat{\mu} | \Psi_i \rangle dz \ , \tag{22}$$

where z follows a closed contour which encircles those eigenvalues of $\hat{H}$ that are lower than E_i (see Fig. 2).

By evaluating the partial rates for decay to individual electronic states, we defined the integration curve from the two quantities T' and V_e'': the energy of the decaying level and the minimum potential energy of the final electronic state. We found that a circle centered at V_e'' and going through T' gave very accurate results. The sum-over-states approach requires a reasonably accurate eigenfunction for every contributing state, and any continuum contribution must be evaluated by integration over continuum states. In the HeH case, radiative transitions to the dissociative X state cannot be treated by the sum-over-states approach, except possibly with a very large effort in evaluating wave functions. In contrast, the integral in Eq. (22) can usually be evaluated with excellent precision using, as suggested in Fig. 2, a small number of complex points.

This scheme requires that an inhomogeneous radial Schrödinger equation

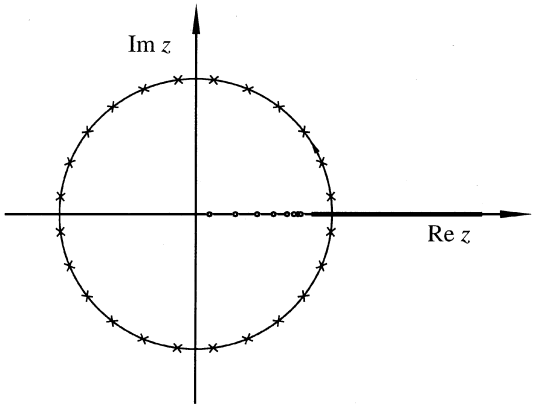

Fig. 2. The integration contour used in Eq. (22). The *crosses* mark the points used for numerical integration. The *small rings* show typical positions for bound states, while the *fat line* marks a continuum

$$(\hat{H}_a - z)\psi_\epsilon = \mu(R)\chi_i(R) \tag{23}$$

is solved for each complex value z used in the integration, where $\hat{H}_a$ denotes the Hamiltonian in the adiabatic approximation. Complex conjugation is used to bring down the number of z values, and the equations are solved quite efficiently by the preconditioned conjugate gradient (PCG) method.

Non-radiative transition rates were computed statically from the Golden Rule expression using matrix elements over the adiabatic wave functions:

$$\tau^{-1} = \tau_0^{-1} \sqrt{\frac{2M}{T' - V_\infty''}}\, 4 \left| \langle \psi_\epsilon | \hat{H}_{na} | \chi_i \rangle \right|^2. \tag{24}$$

Here, the function ψ_ϵ is a continuum wave function, evaluated on the lower adiabatic potential, using the same energy T' as the decaying vibrational eigenstate of the upper potential, and normalized to unit amplitude at infinity. The operator $\hat{H}_{na}$ is the non-adiabatic part of the Hamiltonian. The asymptotic kinetic energy ϵ equals the excess energy $T' - V_\infty''$.

The continuum wave function ψ_ϵ is obtained by solving the inhomogeneous equation

$$(\hat{H}_a - T')\psi_\epsilon = \text{RHS}, \tag{25}$$

again by the PCG method. If the right-hand side (RHS) is zero in every grid point except the last, it implies that ψ_ϵ solves the Schrödinger equation with energy T' everywhere except at that grid point. After proper normalization it is used as a continuum orbital.

3 Results and discussion

3.1 Potential functions

At large distances, the exact adiabatic energies are $-1/2n^2$ a.u. below the HeH^+ energy. Our Born-Oppenheimer potential functions were shifted to reproduce these theoretical asymptotic energy differences. This required lowering the HeH potential functions by 0.1 cm^{-1} for the X state (1*s*), 15 cm^{-1} for states A, B, and C (2*s* and 2*p*), while for the $n = 3$ asymptotes different shifts were applied: 4 cm^{-1} for the dissociation to 3*s*(D), 14 cm^{-1} for the F and E states (3*p*), and 92 cm^{-1} for the G, H, and I states (3*d*).

Apart from these shifts, no further scaling was done. The resulting asymptotic energy differences should now be close to the experimental hydrogenic excitation energies if we compute the adiabatic corrections properly. The dissociation limits for the higher states are 82259 cm^{-1} and 97492 cm^{-1} above the ground state for $n = 2$ and $n = 3$, respectively, and the corresponding adiabatic corrections are -45 and -53 cm^{-1}. These numbers are reproduced to within 1 cm^{-1} by our calculations (see Table 1).

Adiabatic corrections to the Born-Oppenheimer wave functions were computed for the six lowest states of HeH (X, A, B, C, D, and E), whereas for the higher ones (F, G, and H) and for the HeH^+ ground state only Born-

Oppenheimer wave functions were determined. The adiabatic corrections and other matrix elements were computed from RASSCF wave functions. In this simple system, these are accurate enough. The spectroscopic constants derived from the MRCI and from the RASSCF potential functions are nearly the same. The R_e values differ by about 0.003 a_0, and the harmonic vibration energies by about 10 cm^{-1}.

The ^{4}HeH and ^{4}HeD isotopomers were considered in the present study. A total of 212 bound states was obtained, with $v = 0 \ldots 3$ for the C state and $v = 0 \ldots 4$ for the others, and $N \leq 7$.

The potential function parameters and the spectroscopic constants derived from rovibrational levels are shown in Tables 1, 2, and 3. The equilibrium constants were obtained by fitting Dunham parameters in the so-called R representation.

$$E(v,N) = \sum_{kl} Y_{kl}(v+1/2)^k (N(N+1) - \Lambda^2)^l \,, \qquad (26)$$

where the levels with $v = 0, 1, 2$ and $N = \Lambda, \Lambda+1, \Lambda+2$ were used in the fit.

For the HeH^+ and HeD^+ isotopic species spectroscopic constants obtained here at the Born-Oppenheimer level of approximation are compared with those of previous high-quality calculations by Kolos and Peek [28] and Bishop and Cheung [29] in Tables 2 and 4, and the agreement is found to be very good. Although the

Table 1. HeH potential function parameters with and without adiabatic correction. (*Ad* including adiabatic correction, *BO* Born-Oppenheimer potential)

State	Source	V_∞ a.u.	V_∞ rel X cm^{-1}	D_e cm^{-1}	R_e a_0	ω_e cm^{-1}	Barrier cm^{-1}	R_{Barr} a_0
HeH^+ X	BO	−2.9024123		16465.6	1.4637	3221.2		
HeH X	Ad	−3.4017415	0	3.9	6.83	28.6		
	BO	−3.4024123		3.9	6.83	28.6		
A	Ad	−3.0269455	82258	20614.3	1.4005	3682.8		
	BO	−3.0274123		20660.6	1.3993	3681.7		
B	Ad	−3.0269459	82258	17700.2	1.4527	3312.4		
	BO	−3.0274123		17783.7	1.4511	3317.2		
C	Ad	−3.0269429	82259	7762.7	1.5313	2933.3	13193.1	3.97
	BO	−3.0274123		7841.8	1.5295	2934.2	13258.1	3.97
D	Ad	−2.9575390	97491	17472.5	1.4451	3357.1		
	BO	−2.9579678		17521.3	1.4442	3357.1		
E	Ad	−2.9575394	97491	16745.1	1.4573	3321.4		
	BO	−3.0348846		16881.3	1.4599	3253.2		
F	BO	−2.9579678		16548.1	1.4667	3197.5	16601.9	12.1

Table 2. HeH spectroscopic constants (cm^{-1}) with and without adiabatic corrections. (*BC* using data from Bishop and Cheung [29], *Exp* Ketterle et al. [15], *Kolos* using the potential of Kolos and Peek [28], *vHP* van Hemert and Peyerimhoff [14])

State	Source	Y_{10} (ω_e)	Y_{20} $(-\omega_e x)$	Y_{01} (B_e)	Y_{11} $(-\alpha_e)$	Y_{02} $(-D_e)$	R_e/a_0
HeH^+ X	BO	3219.2	−153.6	34.89	−2.69	−0.0164	1.4637
	BC	3218.3	−153.5	34.91	−2.70	−0.0164	
	Kolos	3218.6	−153.5	34.91	−2.70	−0.0164	1.4632
A	Ad	3707.3	−153.7	38.11	−2.61	−0.0161	1.4005
	BO	3705.8	−153.5	38.17	−2.60	−0.0162	1.3993
	vHP	3670.1	−154.3	37.40	−2.45	−0.0150	1.4139
	Exp	3718	−161	37.90	−2.61	−0.0156	1.4003
B	Ad	3319.8	−151.6	35.45	−2.62	−0.0161	1.4527
	BO	3326.3	−151.6	35.53	−2.63	−0.0161	1.4511
	vHP	3226.9	−145.2	34.60	−2.55	−0.0150	1.4701
C	Ad	2904.2	−140.6	31.89	−2.54	−0.0153	1.5313
	BO	2905.9	−140.2	31.97	−2.55	−0.0154	1.5295
	vHP	2877.1	−137.7	31.43	−2.49	−0.0146	1.5424
	Exp	2902	−140.6	31.84	−2.67	−0.0147	1.5324
D	Ad	3313.5	−114.4	35.71	−2.48	−0.0174	1.4451
	BO	3364.5	−160.0	35.81	−2.60	−0.0164	1.4442
	vHP	3346.0	−167.3	35.23	−2.66	−0.0154	1.4569
E	Ad	3365.9	−191.7	35.39	−2.88	−0.0148	1.4573
	BO	3251.8	−154.2	35.10	−2.68	−0.0163	1.4599
	vHP	3174.2	−143.3	34.42	−2.66	−0.0158	1.4739
F	BO	3185.1	−147.4	34.77	−2.78	−0.0163	1.4667
	vHP	3148.5	−141.1	34.13	−2.66	−0.0155	1.4802
$1^2\Delta$(G)	BO	3237.0	−154.4	35.08	−2.70	−0.0163	1.4624
	vHP	3195.1	−154.3	34.33	−2.66	−0.0154	1.4758

differences in absolute energies can be as large as 278.2 cm^{-1} for the $vJ = 00$ level, relative energy differences turn out to be very small. Our fundamental frequency of $v_0 = 2912.08\ cm^{-1}$ differs by only 0.12 cm^{-1} and the dissociation energy D_0 of 14890.9 cm^{-1} exceeds the reference value by 9.7 cm^{-1}.

The HeH ground state is strongly repulsive, with a weak van der Waals minimum of 3.9 cm^{-1} (Experiment: 3.7 [32]). The A state is not very well characterized experimentally, owing to its very rapid predissociation to the ground state. As we shall see, the levels are broadened by many reciprocal centimeter units, and Ketterle et al. [15] estimate an error bar of 14 cm^{-1} for the harmonic frequency. The C state is better characterized. The D and E states show large adiabatic correction effects. For the D state, this correction has a high peak around $2.2a_0$. From the adiabatic MRCI potential energies, this can be seen to be caused by an avoided crossing with the F state, with estimated diabatic energy gap of roughly $940(R - 2.19a_0)$ cm^{-1} and an interaction matrix element of 80 cm^{-1}. The large and peaked contribution to the energy curve gives, in particular, a too low anharmonicity. Since we lack the matrix elements with the differential F state wave function, this cannot be corrected by proper diabatization.

Table 3. HeH rotational constants (cm^{-1}). (for abbreviations, see Table 2)

State	Source	T_0	B_0	D_0
A	Ad	0	36.80	0.0158
	vHP	0	36.68	
	Exp	0	36.53	0.0145
B	Ad	2650.5	34.16	0.0159
	vHP	2921.3	33.33	
	Exp	2563.3	34.18	0.0158
C	Ad	12455.0	30.62	0.0151
	vHP	12262.6	30.18	
	Exp	12488.0	30.50	0.0143
D	Ad	18203.4	34.48	0.0158
	vHP	18085.0	33.90	
	Exp	18212.8	33.28	0.0179
E	Ad	18838.1	33.98	0.0158
	vHP	18764.8	33.09	
	Exp	18762.0	33.69	0.0141

Except for the A and C states, there are no experimental vibration data, and comparison to experiment is limited to relative term values and rotational constants for the 0-0 transition. We compare to the deperturbed parameters T, B_0, and D_0 of Refs. [15, 30, 31]. The term values are relative to the A state and depend on the assumed A-B term difference of 2650.5 cm^{-1}. Because of the width of the A levels, the experimental T_0 values are less accurate than the differences. Note that term values for the B and E states refer to a non-existing $N = 0$ level: T_0 is obtained by fitting the conventional formula $T_0 + B_0M - D_0M^2$ with $M = N(N + 1)$ to the lowest rotational levels.

3.2 Radiative and non-radiative rates

The total widths computed for the lowest non-rotational levels of the A, C, and D states are summarized in Table 5 and partial radiative rates for their decay to the X state together with the total radiative lifetimes τ_0^{rad} of these states are collected in Table 6. A more detailed account of the radiative and non-radiative decay rates, with the partial rates of final electronic states, can be found in Tables 7–9.

The fast predissociation of the A state is well-established by experiment and theory. The experimental numbers are quite uncertain: Ketterle et al. [15] give estimated widths of 3.1 ± 1 cm^{-1} for rotational quantum numbers $N < 5$ and 1.2 cm^{-1} for $N > 5$ for the vibrational ground state of ^{4}HeH. For the HeD species, the corresponding numbers are 1.1 cm^{-1}($N < 5$) and 0.5 cm^{-1}. For HeD, they also give the width for the states with $v = 1$ and $N > 5$, namely 2.0 ± 1 cm^{-1}. (The uncertainty in these numbers is ± 0.4 cm^{-1}, unless stated otherwise). All calculations give a linewidth for the rotationless $v' = 0$ state of about 3–5 cm^{-1}, which increases rapidly with vibrational excitation, and gradually decreases for larger N. The experimental data indicate slightly smaller widths and a stronger dependence on N than most calculations.

The diabatic coupling of the A and X states at small distances is so large that at least a two-states coupled channel treatment would be preferable. This is also the case for the coupling between the C and D states, which

Table 4. HeD spectroscopic constants (cm^{-1}) with and without adiabatic corrections. (for abbreviations see Tables 1 and 2)

State	Source	Y_{10} (ω_e)	Y_{20} ($-\omega_e x$)	Y_{01} (B_e)	Y_{11} ($-\alpha_e$)	Y_{02} ($-D_e$)
HeD^+ X	BO	2495.7	−92.3	20.97	−1.28	−0.0059
	Kolos	2495.2	−92.2	20.98	−1.27	−0.0059
A	Ad	2872.9	−91.99	22.92	−1.22	−0.0058
	BO	2871.9	−91.9	22.94	−1.22	−0.0059
B	Ad	2574.9	−91.0	21.32	−1.23	−0.0058
	BO	2577.6	−91.1	21.34	−1.23	−0.0058
C	Ad	2253.8	−85.0	19.18	−1.19	−0.0055
	BO	2254.7	−85.0	19.21	−1.19	−0.0055
D	Ad	2583.2	−78.4	21.54	−1.30	−0.0059
	BO	2603.8	−94.5	21.53	−1.23	−0.0059
E	Ad	2579.4	−109.3	21.15	−1.21	−0.0056
	BO	2519.9	−92.6	21.08	−1.25	−0.0059
F	BO	2474.1	−90.4	20.89	−1.29	−0.0059
$1^2\Delta$(G)	BO	2506.0	−92.7	21.05	−1.26	−0.0059

Table 5. Total widths (cm^{-1}) of A, C, and D states with $N = 0$ of HeH and HeD. *PTB* Petsalakis et al. [13], *vHP* van Hemert and Peyerimhoff [14], *VN* Vegiri and Nicolaides [33], *V* Vegiri [16]

State	Source	$v' = 0$	1	2	3	4
	PTB	4.3	11.6	20.9	28.4	34.5
HeH A	vHB	5.1	15.0	25.0		
	VN	4.4	11.9	22.2	28.2	31.7
	This work	5.07	16.0	27.8	37.4	44.3
HeD A	vHP	1.2	4.0	8.0		
	This work	1.20	3.94	11.5	6.88	
	PTB	0.0054	0.0239	0.0277	0.0228	0.0013
HeH C	VN	0.011	0.083	0.32	0.80	0.63
	V	0.023	0.055	0.209	–	0.303
	This work	0.00047	0.00096	0.0018	0.0030	
HeD C	V	–	0.002	0.007	0.009	0.032
	This work	0.00034	0.00051	0.00053	0.00091	
	PTB	0.0080	0.0080	0.0113	0.0133	0.0131
HeH D	VN	0.0024	0.113	1.75	21.1	20.5
	V	$<10^{-5}$	0.48			
	This work	0.0013	0.0046	0.0115	0.0149	0.0212
HeD D	V	0.007	0.016	0.044		
	This work	0.00017	0.0214	0.0015	0.94	0.58

Table 6. Partial radiative rates/ 10^6 s^{-1} for decay to the X electronic state, and the total radiative lifetime τ_0^{rad}. (*PTB* Petsalakis et al. [13]

		$v' = 0$	1	2	3	τ_0^{rad} (ns)
A → X	PTB	22.8	31.2	39.2	47.1	43.8
	This work	18.6	26.4	34.0	41.7	53.8
B → X	PTB	56.0	74.8	97.5	124.0	17.8
	This work	62.5	82.3	107.0	137.0	15.9
C → X	PTB	43.6	48.7	54.6	61.8	15.2
	This work	36.8	40.8	45.7	52.5	16.1
D → X	PTB	12.4	16.1	20.3	25.6	39.3
	This work	13.6	22.8	37.9	53.9	32.5
E → X	PTB	8.0	14.0	21.7	31.3	31.0
	This work	0.7	0.4	1.2	1.9	52.4

allows D levels that are below the D asymptote to predissociate by coupling to continuum C states, giving $n = 2$ H atoms as a product. The extreme predissociation rate can be expected to show a larger difference between static and coupled channel calculations, but this does not seem to be the case. The Golden Rule results of Petsalakis et al. [13, 34] are slightly lower than our widths which agree well with coupled channel calculations [14, 33].

A very accurate full coupled channel treatment of the six lowest HeH states was recently performed by Vegiri [16], whereas van Hemert and Peyerimhoff [14] have concentrated on two-states coupled channel calculations for the X/A and C/D states. In the latter study the couplings between the C/D states were not computed for energies above the C state asymptote. Predissociation widths are thus only obtained for the A state. The results are in good agreement with experiment. Samples of the necessary matrix elements are tabulated in the paper, and these agree well with ours. By an *R*-dependent scaling procedure to correct the potential curves, they are able to bring their final rotation-vibration levels into almost perfect agreement with experiment. The effect of the C/D coupling on level shifts is pronounced for some levels.

For the X/A coupling, an interesting approach is that of Honigmann et al. [35]. They use quadrupole matrix elements to define quasidiabatic wave functions, and assume that all derivative couplings are negligible in this basis. Furthermore, they use a complex dilation method to obtain resonances. The widths they obtain for the A states are the smallest reported: about 3 cm^{-1} for the lowest A level. These values are still not unreasonable, and are in fact in better agreement with experiment than most other calculations. However, with no independent way of assessing the approximation of neglecting derivative couplings in the quasidiabatic basis, it should not be compared with other studies.

For non-rotational states, Vegiri and Nicolaides [33] studied the predissociation of the A, C, and D states using multistate coupled channel calculations (called multistate approach). Predicted C widths are quite different from ours which is essentially due to the more general treatment applied in that study. This can also be seen from comparison of the multistate results with those of an earlier calculation by Petsalakis et al. [13] where both studies use the same matrix elements as an input but arrive at different results. A more complete multistate calculation was performed by Vegiri [16] in which rotational couplings and higher N quantum numbers were also included. Obviously the more elaborate treatment has a strong effect on the widths which largely explains the differences to the results of the present study which were obtained from the Golden Rule formula. However, there is also disagreement between the present results and other Golden Rule results of Refs. [13, 34] which can only be explained by the fact that the coupling matrix elements used in these calcu-

Table 7. Radiative decay rates from the states A, C, and D partitioned by final electronic state. Units are 10^6 s^{-1}

	v'	$N'=0$	1	2	3	4	5	6	7
A → X	0	18.6	18.7	18.9	19.1	19.5	19.9	20.5	21.1
	1	26.4	26.5	26.7	26.9	27.3	27.7	28.3	28.9
	2	34.0	34.1	34.3	34.6	34.9	35.4	36.0	36.6
	3	41.7	41.8	42.1	42.4	42.8	43.3	43.9	44.7
	4	50.1	50.2	50.5	50.8	51.3	51.9	52.7	53.6
C → X	0	36.8	36.9	36.9	37.1	37.2	37.4	37.7	38.0
	1	40.8	40.8	40.9	41.1	41.3	41.6	41.9	42.3
	2	45.7	45.8	45.9	46.2	46.4	46.8	47.3	47.8
	3	52.5	52.6	52.8	53.1	53.6	54.2	54.9	55.7
C → A	0	23.8	23.8	23.8	23.7	23.7	23.6	23.5	23.3
	1	21.0	20.9	20.9	20.8	20.8	20.7	20.6	20.4
	2	18.3	18.3	18.3	18.2	18.1	18.0	17.9	17.8
	3	16.0	15.9	15.9	15.8	15.8	15.7	15.5	15.4
C → B	0	1.4	1.4	1.4	1.4	1.4	1.3	1.3	1.2
	1	1.3	1.3	1.2	1.2	1.2	1.2	1.1	1.1
	2	1.2	1.2	1.2	1.2	1.1	1.1	1.1	1.0
	3	1.2	1.2	1.2	1.2	1.2	1.2	1.2	1.1
D → X	0	13.6	13.7	13.8	14.0	14.2	14.6	15.0	15.5
	1	22.8	22.9	23.2	23.5	24.0	24.7	25.4	26.4
	2	37.9	38.0	38.4	39.0	39.7	40.7	41.8	43.2
	3	53.9	54.1	54.4	54.8	55.4	56.1	56.8	57.7
	4	69.2	69.4	60.2	60.4	60.8	71.8	72.9	74.1
D → A	0	4.4	4.4	4.4	4.3	4.2	4.1	4.0	3.9
	1	3.6	3.5	3.5	3.5	3.4	3.3	3.2	3.1
	2	3.3	3.3	3.3	3.3	3.3	3.2	3.2	3.2
	3	3.4	3.4	3.4	3.4	3.3	3.3	3.2	3.1
	4	2.4	2.4	2.8	2.8	2.8	2.2	2.1	2.0
D → B	0	11.3	11.3	11.3	11.3	11.4	11.4	11.5	11.5
	1	13.2	13.2	13.3	13.4	13.5	13.7	13.9	14.1
	2	17.9	17.9	18.0	18.2	18.5	18.8	19.1	19.5
	3	22.1	22.1	22.1	22.2	22.2	22.2	22.2	22.2
	4	20.4	20.4	20.8	20.8	20.8	20.2	20.0	19.9
D → C	0	1.5	1.5	1.5	1.5	1.5	1.5	1.6	1.6
	1	1.0	1.0	1.0	1.0	1.0	1.0	0.9	0.9
	2	0.8	0.8	0.9	0.9	1.0	1.1	1.3	1.6
	3	6.0	6.1	6.3	6.5	6.8	7.1	7.4	7.8
	4	10.5	10.5	8.2	8.2	8.2	10.7	10.8	10.8

lations are different. To some extent this also affects the disagreement with the multistate results of Refs. [16, 33]. The matrix elements used there were actually taken from two different sources: rotational couplings from van Hemert and Peyerimhoff [14] and transition moments and radial couplings from Refs. [17, 18].

The transition moments collected in Table 5 of Ref. [17] and in Table 4 of Ref. [18] are in obvious disagreement with the present calculations. The magnitude and the R dependences of the X-E and C-E transition moments are different and there appear to be sign errors in the C-A, D-C, and C-B moments of Ref. [18]. The non-adiabatic matrix elements in Ref. [18] also seem to have some inconsistent signs. We suggest that the X-A, X-C, and X-D columns have the wrong sign for d/dR at $3a_0$ such as the A-D values for R values less than $1a_0$. The d^2/dR^2 elements are less easy to compare, since the authors collect matrix elements of the type $\langle d/dR|d/dR\rangle$ under this heading (see the note in Ref. [30] of Ref. [31]).

The matrix elements of Petsalakis et al. have been used in several later studies. Petsalakis and coworkers used them to compute radiative and non-radiative rates [13]. Their Table 1 gives radiative rates for transitions from the A, C, and D $N=0$ states and from the B and E $N=1$ states, with $v=0\ldots5$, to the X state. Their rates for the states A to D are quite similar to ours except that our D rates have a faster increase with v' (see Table 6).

The E → X rates of Ref. [13] are 10–30 times larger than ours. This appears, however, to be due to the different definition of the states. Their states are diabatic and at shorter distances the X state is thus a mixture of adiabatic X and A states with the effect that their E → X transition rates borrow intensity from the E → A rates. The total radiative lifetimes reported in Ref. [13] are not too different from ours, which means that the dominant E-A transitions are computed with similar rates.

Differences in the non-radiative rates are more difficult to trace back. These rates are very sensitive to details of the vibrational wave functions and of the matrix elements. The predissociation rates derived in other studies for the C state are quite different from ours and this is also true for the lowest vibrational levels of the D state. Apart from obvious reasons for some of the disagreements so that a multistate calculation is actually needed to determine reliable non-radiative rates, an additional source for the discrepancies is the apparent differences in the matrix elements used in these calculations.

Table 8. Radiative decay rates from the states B, E, and G partitioned by final electronic state. Units are 10^6 s^{-1}

	v'	$N' = 1$	2	3	4	5	6	7
B → X	0	62.5	62.9	63.4	64.2	65.1	66.3	67.7
	1	82.3	82.8	83.5	84.5	85.8	87.4	89.2
	2	106.8	107.5	108.5	109.8	111.5	113.6	116.1
	3	137.3	138.1	139.5	141.3	143.6	146.4	149.7
	4	175.3	176.5	178.3	180.7	183.8	187.6	192.1
B → A	0	0.3	0.3	0.2	0.2	0.2	0.2	0.2
	1	0.2	0.2	0.2	0.2	0.2	0.2	0.2
	2	0.2	0.2	0.2	0.2	0.2	0.2	0.2
	3	0.1	0.1	0.1	0.1	0.1	0.1	0.1
	4	0.1	0.1	0.1	0.1	0.1	0.1	0.1
E → X	0	0.7	0.7	0.7	0.8	0.8	0.8	0.8
	1	0.4	0.4	0.4	0.4	0.4	0.4	0.5
	2	1.2	1.2	1.2	1.3	1.3	1.4	1.4
	3	1.9	1.9	1.9	1.9	1.9	1.9	2.0
	4	2.0	2.0	2.0	2.0	2.0	2.0	2.0
E → A	0	11.1	11.1	11.1	11.0	11.0	10.9	10.8
	1	8.6	8.6	8.5	8.4	8.3	8.2	8.1
	2	6.8	6.7	6.7	6.7	6.6	6.6	6.5
	3	6.0	5.9	5.9	5.9	5.9	5.8	5.8
	4	5.6	5.6	5.6	5.6	5.6	5.6	5.7
E → B	0	3.4	3.4	3.5	3.7	3.8	4.0	4.3
	1	9.3	9.4	9.6	9.8	10.2	10.6	11.0
	2	15.1	15.2	15.4	15.6	15.8	16.1	16.5
	3	18.8	18.8	19.0	19.2	19.4	19.6	19.9
	4	21.7	21.8	21.9	22.0	22.2	22.4	22.7
E → C	0	3.8	3.8	3.9	3.9	4.0	4.1	4.2
	1	5.6	5.7	5.7	5.8	5.9	6.0	6.2
	2	7.1	7.2	7.2	7.3	7.4	7.4	7.5
	3	8.0	8.1	8.1	8.2	8.2	8.3	8.4
	4	8.6	8.7	8.7	8.7	8.7	8.8	8.8
G → B	0		34.5	34.6	34.6	34.6	34.6	34.6
	1		34.5	34.5	34.5	34.5	34.5	34.5
	2		34.3	34.3	34.4	34.4	34.4	34.4
	3		34.2	34.2	34.2	34.2	34.2	34.2
	4		34.0	34.0	34.0	33.9	33.9	33.9

Table 9. Non-radiative decay rates from the states A, B, D, and E partitioned by final electronic state. Units are 10^{10} s^{-1}

	v'	$N' = 0$	1	2	3	4	5	6	7
A → X	0	95.6	105.8	103.9	97.7	83.2	86.3	77.9	91.2
	1	301.4	296.7	295.4	275.7	260.2	243.1	225.1	203.3
	2	523.2	517.0	496.9	475.8	452.7	431.2	389.4	358.9
	3	704.7	698.9	687.7	665.3	616.7	572.3	544.6	485.7
	4	833.9	818.7	795.7	752.7	710.3	679.6	637.1	564.6
D → X	1	0.1	0.1	0.1	0.1	0.1	0.1	0.1	0.1
	2	0.2	0.2	0.2	0.2	0.1	0.1	0.1	0.1
	3	0.3	0.3	0.2	0.2	0.2	0.2	0.2	0.2
	4	0.4	0.4	0.3	0.3	0.3	0.3	0.3	0.9
D → C	2	0.0	0.0	1.4	0.2	3.2	1.5	0.1	1.4
	3	0.0	1.4	0.7	0.2	2.0	0.2	0.1	10.3
	4	0.0	3.8	10.1	0.3	0.2	5.5	0.1	0.7
B → X	0		0.0	0.0	0.0	0.1	0.1	0.1	0.1
	1		0.0	0.1	0.1	0.2	0.3	0.4	0.5
	2		0.0	0.1	0.3	0.6	0.6	0.7	0.9
	3		0.1	0.2	0.4	0.6	0.8	1.0	1.2
	4		0.1	0.2	0.4	0.7	0.9	1.2	1.5
E → C	1		0.0	0.0	0.0	0.0	0.0	0.1	0.0
	3		0.0	0.3	1.9	1.2	0.7	11.7	0.9
	4		0.1	0.3	1.0	1.2	5.9	2.0	1.0

3.3 Predissociation yields

The radiative rates in Tables 7 and 8 depend rather smoothly on v' and N', whereas their non-radiative counterparts collected in Table 9 show a less regular dependence. This is essentially caused by resonances, and their positions and strengths depend sensitively on several details of the calculation. For the A → X transitions the radial coupling matrix element multiplied by the initial state wave function is largest at quite short distances close to the Franck-Condon point. The continuum wave function starts to oscillate very rapidly

after its first maximum. Thus the main contribution to the transition rate comes from the size of the initial wave function at a point somewhere on its left tail beyond the turning point unless v' is very high. This explains the regular and rapid increase with v' and the gradual, roughly parabolic decrease with N' of this rate.

Other rates have a more complicated behavior in their dependence upon wave functions and matrix elements. Pronounced resonances can occur in the static approximation for decays to the C state at energies close to the quasibound states. For this type of calculation, the resonances are caused by a blowup (or, rarely, a shrinking) of the inner part of the wave function inside the barrier when imposing normalizing conditions on the asymptotic part. Such resonances occur, for example, for the ^{4}HeH species for the D state with $v = 2, N = 4$, but particularly for several of the ^{4}HeD D states, for example, $v = 1, N = 5; v = 3, N = 0,\ 1$; and $v = 4, N = 0,\ 3$.

Our calculations are incomplete in that the direct predissociation of higher C state levels by tunneling through the barrier has not been studied. The rates for D states coupling to the C state above the C dissociation limit are still valid, although within the static (Golden Rule) picture. However, level shifts of the stronger resonances will change the appearance of these resonances, and a detailed description will not be valid without including at least the C/D coupling already in the determination of the wave functions.

Recent experiments by Semaniak et al. [36] and Strömholm et al. [37] show that capture of low-energy electrons results in mainly H ($n=2$) atoms. States with $\Lambda > 1$ can be assumed to decay only via processes that lower Λ. At the end of the decay chain, it is natural for $\Lambda = 1$ to yield H ($n=2$), since this is the dissociation product of the lowest II state. However, the Σ states could go via the A state, which would immediately (in 0.1 ps or less) go to the X state and produce high-velocity H 1s atoms. We conclude that the processes that convert electronic energy to nuclear kinetic energy must have avoided this route. Two theoretical calculations give different results: Sarpal et al. [38] predict production of H 1s atoms, while Guberman [39] predicts $n = 2$ products, in agreement with experiments.

Our results say nothing about the initial steps in the electron capture process. However, for the capture of low-energy electrons by HeH^+ X state ions, some trends can be derived based on simple energy conservation considerations. The initial state has an energy slightly above the HeH^+ ground state. The rotational quantum number N^+ of the ion is of course small, but not much can be said about the l quantum number of the electron. Thus, initially we have a reasonably well defined energy, but the rotational quantum number N of the neutral HeH state formed will be distributed over a fairly wide range. The D state and all the higher ones have asymptotes above the HeH^+ X state. For the D state, the available energy implies that primarily the $v = 4$ level is populated. Our results show that a bound D state with $v = 4$, with any realistic distribution of initial N, will produce primarily a decaying C state. This is thus a plausible last step in the DR and is in full agreement with experimental findings and with the theoretical results of Ref. [39].

4 Summary and conclusions

This paper is the first study of the DR process. Potential curves have been obtained for the ten lowest states of HeH: those that dissociate to H atoms with $n = 1, 2$, and 3. For the six states X up to E, all matrix elements have been evaluated to allow full multistate coupled channel calculations, and also those matrix elements coupling these with the remaining higher states G, H, and I. However, at this stage, only uncoupled calculations have been done.

The resulting spectroscopic constants agree very well with experimental results, where these are available. The predissociation widths and yields, computed from the adiabatic wave functions by the Golden Rule, are in some cases in marked disagreement with other recent calculations. This is explained by the different matrix elements. Many of the values we have computed are in disagreement with the currently most used set of data. Our matrix elements are available on request for further studies.

The calculated yields are in agreement with recent experimental results. It seems likely that a common final step is predissociation of the D state, with $v' \approx 4$, to produce a dissociating C state which yields excited H atoms with $n = 2$.

The matrix elements missing from this study are those that couple the higher states, G, H, and I, with each other, and thus also the diagonal elements needed for adiabatic correction of the potential curves. We intend to complement this paper by a forthcoming study where these elements are also included, and also to make a full coupled channel calculation involving all ten lowest states. However, we do not anticipate any major change in the results, except of course those that involve certain resonances.

However, a greater concern is to study the full electron capture process. It does not seem very profitable to extend the present study to include the $n = 4$ manifold. Instead, we are presently writing programs that allow the description of the full capture and dissociation process in terms of coupled one-electron problems. This approach will be necessary for larger systems.

Acknowledgements. The research reported in this paper was conducted at the Max Planck Institute of Astrophysics in Garching. P.-Å.M. was a visitor at the institute and is grateful for the hospitality and financial support that he received.

References

1. Bates DR, (1950) Phys Rev 78: 492
2. Bardsley JN (1968) J Phys B 1: 349
3. Bardsley JN, Biondi MA (1970) Adv At Mol Phys 6: 1
4. Bates DR (1992) J Phys B 25: 5479
5. Michels HH, Harris FF (1963) J Chem Phys 39: 1464
6 Michels HH, Hobbs RH (1984) Astrophys J 286: L27
7. Kraemer WP, Hazi AU (1989) In: Mitchell JBA, Euberman SL (eds): Dissociative recombination: theory, experiment and applications. World Scientific, Singapore, pp 61
8. Bates DR (1994) Adv At Mol Phys 34: 427
9. Bardsley JN (1968) J Phys B 1: 365
10. O'Malley TF (1981) J Phys B 14: 1229
11. Hickman AP (1987) J Phys B 20: 2091

12. Meyer W, Frommhold L (1994) Theor Chim Acta 88: 201
13. Petsalakis ID, Theodorakopoulos G, Buenker RJ (1988) Phys Rev A 38: 4004
14. Van Hemert MC, Peyerimhoff SD (1991) J Chem Phys 94: 4369
15. Ketterle W, Dodhy A, Walther H (1988) J Chem Phys 89: 3442
16. Vegiri A (1996) J Phys B 29: 3611
17. Theodorakopoulos G, Petsalakis ID, Nicolaides CA, Buenker RJ (1987) J Phys B 20: 2339
18. Petsalakis ID, Theodorakopoulos G, Nicolaides CA, Buenker RJ (1987) J Phys B 20: 5959
19. Andersson K, Fülscher MP, Karlstrom G, Lindh R, Malmqvist P-Å, Olsen J, Roos BO, Sadlej J, Blomberg MRA, Siegbahn PEM, Kello V, Noga J, Urban M, Widmark PO (1994) MOLCAS, Version 3. University of Lund, Lund, Sweden
20. Siegbahn PEM (1980) J Chem Phys 72: 1647
21. Olsen J, Roos BO, Jørgensen P, Jensen HJA (1988) J Chem Phys 89: 2185
22. Malmqvist P-Å, Rendell A, Roos BO (1990) J Phys Chem 94: 5477
23. Malmqvist P-Å (1986) Int J Quantum Chem 30: 479
24. Malmqvist P-Å, Roos BO (1989) Chem Phys Lett 155: 189
25. Andersson K, Blomberg MRA, Fülscher MP, Kellö V, Lindh R, Malmqvist P-Å, Noga J, Olsen J, Roos BO, Sadlej AJ, Siegbahn PEM, Urban M, Widmark P-O, (1992) *MOLCAS*, version 2. University of Lund, Lund, Sweden
26. Light JC, Hamilton IP, Lill JV (1985) J Chem Phys 82: 1400
27. Light JC, Whitnell RM, Park TJ, Choi SE (1989) In: A. Lagana (ed) Supercomputer algorithms for reactivity, dynamics and kinetics of small molecules. Kluwer, Boston, p 187
28. Kolos W, Peek JM (1976) Chem Phys 12: 381
29. Bishop DM, Cheung LM (1979) J Mol Spectrosc 75: 462
30. Ketterle W (1990) J Chem Phys 93: 3752
31. Ketterle W (1990) J Chem Phys 93: 3760
32. Toennis JP, Welz W, Wolf G (1976) Chem Phys Lett 44: 5
33. Vegiri A, Nicolaides CA (1995) J Phys B 28: 2927
34. Petsalakis ID, Theodorakopoulos G, Buenker RJ (1996) J Chem Phys 92: 4920
35. Honigmann M, Buenker RJ, Hirsch G, Schöttke S (1992) J Phys B 25: 389
36. Semaniak J, Rosén S, Sundström G, Strömholm C, Datz S, Danared H, Ugglas M af, Larsson M, Van der Zande WJ, Amitay Z, Hechtfischer U, Grieser M, Repnow R, Schmidt M, Schwalm D, Wester R, Wolf A, Zaifman D (1996) Phys Rev A 54: R4617
37. Strömholm C, Semaniak J, Rosén S, Danared H, Datz S, Van der Zande W, Larsson M (1996) Phys Rev A 54: 3086
38. Sarpal BK, Tennyson J, Morgan LA (1994) J Phys B 27: 5943
39. Guberman SL (1994) Phys Rev A 49: R4277